Available online at www.sciencedirect.com
ScienceDirect
Journal of Sound and Vibration 324 (2009) 940–953
JOURNAL OF SOUND AND VIBRATION
www.elsevier.com/locate/jsvi

Stability and bifurcations of hysteretic systems subjected to principal parametric excitation

Nobukatsu Okuizumi[a,*], Koji Kimura[b]

[a]*Research Division of Space Structure and Materials, The Institute of Space and Astronautical Science, Japan Aerospace Exploration Agency, 3-1-1 Yoshinodai, Sagamihara, Kanagawa 229-8510, Japan*
[b]*Department of Mechanical and Environmental Informatics, Tokyo Institute of Technology, 2-12-1 Ookayama, Meguro-ku, Tokyo 152-8552, Japan*

Received 2 August 2007; received in revised form 17 June 2008; accepted 15 February 2009
Handling Editor: L.G. Tham
Available online 26 March 2009

Abstract

Dynamic behavior of smooth hysteretic systems subjected to harmonic parametric excitation is investigated. Wen's differential equation model for hysteresis, which can describe a large class of hysteretic systems, is used. Employing the piecewise power series expression for hysteresis proposed in the previous paper, the method of multiple scales is applied for the case of principal parametric resonance to obtain the second-order approximate solutions and their stability. It is shown that the hysteretic systems are unstable inside the principal resonance region but the responses are bounded having symmetric periodic solutions. It is also shown that the systems are stable outside the region even if viscous damping does not exist because of Hopf bifurcation. Numerical integrations are also performed to illustrate the nonlinear resonant characteristics of the systems and confirmed that trivial stationary solutions and stable symmetric periodic solutions in principal resonance region bifurcate to produce a pair of non-symmetric periodic solutions. Stability regions with regard to excitation parameters are also illustrated. The theoretical and numerical results are compared to examine the validity of the present analysis.

1. Introduction

Mechanical and structural systems under severe dynamic loads often exhibit hysteretic characteristics so that the relationship between displacement and restoring force depends on their past histories. Nonlinear dynamics of hysteretic systems need to be understood for the reliability and safety of mechanical and structural systems.

Resonant characteristics and nonlinear phenomena of bilinear or smooth hysteretic systems subjected to external harmonic excitation have been studied by employing averaging method [1], method of harmonic balance [2,3], method of multiple scales [4] and numerical integration [5]. Resonant characteristics of a bilinear hysteretic system subjected to harmonic parametric excitation were investigated with averaging method [6].

*Corresponding author. Fax: +81 42 759 8297.
E-mail address: okuizumi@isas.jaxa.jp (N. Okuizumi).

0022-460X/$ - see front matter © 2009 Elsevier Ltd. All rights reserved.
doi:10.1016/j.jsv.2009.02.029

Bifurcations and chaos of a bilinear hysteretic system subjected to external and parametric periodic impulse were studied in Refs. [7–10]. On the other hand, the behavior of parametrically excited nonlinear systems such as Mathieu's equation with cubic nonlinearity [11–13], Mathieu's equation with quadratic and cubic nonlinearities [14–16] and parametrically excited nonlinear pendulum [17–20] has been widely investigated by theoretical and numerical analyses as well as experiments. It is generally shown that nonlinearity can stabilize unstable Mathieu zones and generate rich bifurcation and chaotic behavior. However, little has been studied on the nonlinear dynamics of smooth hysteretic systems under parametric excitation.

The authors proposed a piecewise power series expression for smooth hysteretic restoring force based on Wen's differential equation model [21,22] which can describe a large class of smooth hysteretic systems [4]. Multiple time scale analysis [23] of the primary and secondary resonance under external harmonic excitation was conducted and the first- and second-order approximate solutions and the systems of differential equations describing the modulation of the amplitudes and phases of the solutions were obtained. Phase plane trajectories, resonance curves and the unstable regions of symmetric solutions obtained from the analyses were compared with the results of numerical integration and the validity of the analysis was confirmed.

In the present paper, multiple time scale analysis of smooth hysteretic systems under principal parametric resonance [16] is performed up to the second order by employing the piecewise power series expression. The differential equations which describe the modulation of the amplitude and phase of the second-order approximate solution are obtained and the stability and bifurcation of a trivial stationary solution is analyzed. Numerical integration is also performed to illustrate the nonlinear response and stability regions of the system and the validity of the analysis is examined.

2. Equations of motion

By using Wen's differential model, the equation of motion for the single-degree-of-freedom hysteretic system subjected to parametric excitation is written as follows [4]:

$$\ddot{x} + \bar{\delta}\dot{x} + (k + \bar{p}\cos 2\omega t)x + z = 0, \tag{1}$$

$$\dot{z} = A\dot{x} - (\bar{\beta}|\dot{x}|z + \bar{\gamma}\dot{x}|z|), \tag{2}$$

where x is the displacement, z is the hysteretic restoring force, $\bar{\delta}$ is the damping coefficient, k is the linear stiffness coefficient, $\bar{p}$ is the amplitude of the parametric forcing, ω is a half of the excitation frequency, and A, $\bar{\beta}$ and $\bar{\gamma}$ are the parameters to control the scale and general shape of hysteretic loop, respectively. Depending on whether $\bar{\beta}+\bar{\gamma}$ is positive or not, this system exhibits softening or hardening hysteretic characteristics, respectively.

3. The piecewise power series expression for hysteretic restoring force

In the following analysis, it is assumed that the displacement of response is described with the periodic solution which contains constant and superharmonic components and that hysteretic restoring force draws a single loop. Fig. 1 illustrates an example of hysteretic loops of periodic solutions. Depending on the signs of velocity $\dot{x}$ and hysteretic restoring force z, hysteretic loop can be divided into four intervals as shown in Fig. 1. Let $t_0,\ldots,t_3$ denote the time for each division point and let $u_0,\ldots,u_3$ denote the displacements at those points. It is also assumed that the nonlinearity of restoring force is weak. Introducing small positive scaling parameter ε, the parameters $\bar{\beta}$ and $\bar{\gamma}$ are replaced by $\varepsilon\beta$ and $\varepsilon\gamma$, respectively. Hysteretic restoring force z can be described with piecewise power series as follows [4]:

$$z = A\left(x - \frac{u_0+u_2}{2}\right) + \varepsilon z_1 + \varepsilon^2 z_2 + O(\varepsilon^3). \tag{3}$$

The coefficients of ε in the expressions of z for intervals (i)–(iv), $z_{11}-z_{14}$, are described as

$$z_{11} = \frac{A}{8}\{(\beta-\gamma)(u_0+u_2)^2 - \beta(u_0-u_2)^2 - 4(\beta-\gamma)(u_0+u_2)x + 4(\beta-\gamma)x^2\}, \tag{4}$$

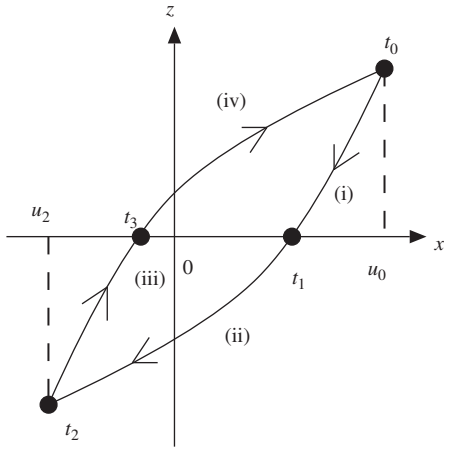

Fig. 1. An example of hysteretic loops divided into four divisions.

$$z_{12} = \frac{A}{8}\{(\beta+\gamma)(u_0+u_2)^2 - \beta(u_0-u_2)^2 - 4(\beta+\gamma)(u_0+u_2)x + 4(\beta+\gamma)x^2\}, \tag{5}$$

$$z_{13} = -\frac{A}{8}\{(\beta-\gamma)(u_0+u_2)^2 - \beta(u_0-u_2)^2 - 4(\beta-\gamma)(u_0+u_2)x + 4(\beta-\gamma)x^2\}, \tag{6}$$

$$z_{14} = -\frac{A}{8}\{(\beta+\gamma)(u_0+u_2)^2 - \beta(u_0-u_2)^2 - 4(\beta+\gamma)(u_0+u_2)x + 4(\beta+\gamma)x^2\}. \tag{7}$$

The times when $z = 0$ are t_1 and t_3 which satisfy the following equations:

$$x(t_1) = \frac{u_0+u_2}{2} + \varepsilon\frac{\beta}{8}(u_0-u_2)^2 + O(\varepsilon^2), \tag{8}$$

$$x(t_3) = \frac{u_0+u_2}{2} - \varepsilon\frac{\beta}{8}(u_0-u_2)^2 + O(\varepsilon^2). \tag{9}$$

Considering the second order of ε, the equation of motion is described as

$$\ddot{x} + \bar{\delta}\dot{x} + (k + A + \bar{p}\cos 2\omega t)x - \frac{A}{2}(u_0+u_2) + \varepsilon z_1 + \varepsilon^2 z_2 = 0. \tag{10}$$

The linear natural frequency of this system is $\sqrt{k+A}$.

4. Multiple time scale analysis

The second-order multiple time scale analysis is applied to the present system (10) in order to obtain approximate solutions and their stability.

4.1. Expansion of the equation of motion

Introducing multiple time scales T_n and their time derivatives D_n, displacement x as well as its maximum and minimum values, u_0 and u_2, are expanded to the power series as follows:

$$T_n = \varepsilon^n t, D_n = \partial/\partial D_n, \quad n = 0, 1, 2, \ldots, \tag{11}$$

$$x = x_0 + \varepsilon x_1 + \varepsilon^2 x_2 + \cdots, \tag{12}$$

$$u_0 = u_{00} + \varepsilon u_{01} + \varepsilon^2 u_{02} + \cdots, \tag{13}$$

$$u_2 = u_{20} + \varepsilon u_{21} + \varepsilon^2 u_{22} + \cdots, \tag{14}$$

where x_0, u_{00} and u_{20} are $O(\varepsilon^0)$, x_1, u_{01} and u_{21} denote $O(\varepsilon^1)$, x_2, u_{02} and u_{22} are $O(\varepsilon^2)$.

Under the assumption that the damping coefficient $\bar{\delta}$ and the excitation amplitude $\bar{p}$ are small, detuning parameter σ for principal parametric resonance is introduced:

$$\bar{\delta} = \varepsilon\delta, \quad \bar{p} = \varepsilon p, \quad k + A - \omega^2 = \varepsilon\sigma. \tag{15}$$

Expanding the equations of motion (10) into the power series of ε and equating the coefficient of each power of ε to zero yield

$$\varepsilon^0 : \ddot{x}_0 + \omega^2 x_0 = \frac{A}{2}(u_{00} + u_{20}), \tag{16}$$

$$\varepsilon^1 : \ddot{x}_1 + \omega^2 x_1 = \frac{A}{2}(u_{01} + u_{21}) - \sigma x_0 - \delta D_0 x_0 - p x_0 \cos 2\omega t - 2D_0 D_1 x_0 - z_1', \tag{17}$$

$$\begin{aligned}\varepsilon^2 : \ddot{x}_2 + 4\omega^2 x_2 = {} & \frac{A}{2}(u_{02} + u_{22}) - \sigma x_1 - p x_1 \cos 2\omega T_0 - D_1^2 x_0 - \delta(D_1 x_0 + D_0 x_1) \\ & - 2D_0 D_2 x_0 - 2D_0 D_1 x_1 - z_2',\end{aligned} \tag{18}$$

where z_1' and z_2', respectively, denote the coefficients of order ε and ε^2 in the expression of z that is obtained by substituting Eqs. (12)–(14) into Eq. (3) and re-expanding z to the power series of ε. z_1' and z_2' are given in piecewise manner.

4.2. First-order approximation

In this section the first-order approximate solution x_0 and the differential equation describing the modulation of the displacement and phase of the solution are derived.

By solving Eq. (16), the first-order solution x_0 is given as follows:

$$x_0 = a\cos(\omega T_0 + \theta) + \frac{A}{2\omega^2}(u_{00} + u_{20}). \tag{19}$$

The times when the displacement reaches its maximum and minimum values, t_0 and t_2 respectively, are obtained as follows:

$$t_0 = -\frac{\theta}{\omega}, \quad t_2 = \frac{\pi}{\omega} - \frac{\theta}{\omega}. \tag{20}$$

Solving equations $x_0(t_0) = u_{00}$ and $x_0(t_2) = u_{20}$ to obtain u_{00} and u_{20} gives the first-order approximate solution as

$$x_0 = a\cos(\omega T_0 + \theta). \tag{21}$$

Substituting Eq. (21) into Eq. (17) yields

$$\begin{aligned}\ddot{x}_1 + \omega^2 x_1 = {} & -z_1' - \sigma a\cos(\omega T_0 + \theta) - pa\cos 2\omega T_0 \cos(\omega T_0 + \theta) \\ & + \delta\omega a \sin(\omega T_0 + \theta) - 2\omega a\cos(\omega T_0 + \theta) D_1\theta - 2\omega \sin(\omega T_0 + \theta) D_1 a.\end{aligned} \tag{22}$$

In order not to produce secular terms, the components of $\cos\omega T_0$ and $\sin\omega T_0$ included in the right-hand side of Eq. (22) should be zero. In this evaluation, zeroth-order approximation of t_1 and t_3 is used which are given by solving Eqs. (8), (9) and (21) as follows:

$$t_1 = \frac{\pi}{2\omega} - \frac{\theta}{\omega}, \quad t_3 = \frac{3\pi}{2\omega} - \frac{\theta}{\omega}. \tag{23}$$

The differential equations governing the modulation of the amplitude and phase of the first-order approximate solution is derived as

$$\dot{a} = \varepsilon D_1 a = \varepsilon\left(-\frac{\delta a}{2} + \frac{pa\sin 2\theta}{4\omega} - \frac{2A\beta a^2}{3\omega\pi}\right), \tag{24}$$

$$\dot{\theta} = \varepsilon D_1 \theta = \varepsilon\left(\frac{\sigma}{2\omega} + \frac{p\cos 2\theta}{4\omega} - \frac{2A\gamma a}{3\omega\pi}\right). \tag{25}$$

4.3. Second-order approximation

In this section, the second-order approximate solution $x_0 + \varepsilon x_1$ and the differential equations which describe the modulation of amplitude a and phase θ of the solution are obtained.

From Eqs. (24) and (25), $D_1 a$ and $D_1\theta$ are derived. Substituting them and z_1' into Eq. (22) gives four differential equations of x_1 corresponding to intervals (i)–(iv). By solving these equations, four solutions with constants of integration are obtained. Making these solutions to be continuous at each division point and not to have components with frequency ω in a whole period, the expressions of x_1 for intervals (i)–(iv), $x_{11}, \ldots, x_{14}$ are obtained.

Substituting x_0 and x_1 into Eq. (18) and formulating the condition of removing secular terms in the same way as in Section 4.2 give the differential equations which describe the modulation of amplitude a and phase θ.

$$\begin{aligned}\dot{a} = {} & \varepsilon\left(-\frac{\delta a}{2} + \frac{pa\sin 2\theta}{4\omega} - \frac{2A\beta a^2}{3\omega\pi}\right) \\ & + \varepsilon^2\left(-\frac{A\delta\gamma a^2}{6\omega^2\pi} + \frac{A\beta\sigma a^2}{3\omega^3\pi} + \frac{A\beta p a^2\cos 2\theta}{40\omega^3\pi} + \frac{A\gamma p a^2\sin 2\theta}{15\omega^3\pi} + \frac{4A^2\beta\gamma a^3}{9\omega^3\pi^2} - \frac{A^2\beta\gamma a^3}{3\omega^3\pi}\right),\end{aligned} \tag{26}$$

$$\begin{aligned}\dot{\theta} = {} & \varepsilon\left(\frac{\sigma}{2\omega} + \frac{p\cos 2\theta}{4\omega} - \frac{2A\gamma a}{3\omega\pi}\right) + \varepsilon^2\left(-\frac{\delta^2}{8\omega} + \frac{3p^2}{64\omega^3} - \frac{\sigma^2}{8\omega^3} + \frac{A\beta\delta a}{6\omega^2\pi}\right. \\ & + \frac{A\gamma\sigma a}{3\omega^3\pi} - n\frac{A\gamma p a\cos 2\theta}{40\omega^3\pi} - \frac{11A\beta p a\sin 2\theta}{60\omega^3\pi} + \frac{7A^2\beta^2 a^2}{48\omega^3} - \frac{5A^2\gamma^2 a^2}{48\omega^3} \\ & \left. - \frac{3A\beta^2 a^2}{16\omega} + \frac{A\gamma^2 a^2}{16\omega} - \frac{26A^2\beta^2 a^2}{27\omega^3\pi^2} + \frac{22A^2\gamma^2 a^2}{27\omega^3\pi^2}\right).\end{aligned} \tag{27}$$

4.4. Stability analysis

Eqs. (24) and (25) or Eqs. (26) and (27) have one trivial solution $a = 0$ which corresponds to $x = 0$ and non-trivial solutions $(a, \theta) = (a_0, \theta_0)$ which corresponds to periodic solutions. In this section, the first-order approximate analysis is demonstrated as follows. The second-order analysis is omitted because it is tedious and qualitatively similar to the first-order analysis.

The stability of non-trivial solutions can be determined by the eigenvalues of Jacobian matrix around equilibrium points in Eqs. (24) and (25). In order to examine the stability of the trivial solution, the next transformation of state variables is useful because fixed value of θ may not be determined for $a = 0$:

$$u = a\cos\theta, \quad v = -a\sin\theta. \tag{28}$$

Applying Eq. (28) to Eqs. (24) and (25) yields

$$\begin{pmatrix}\dot{u}\\ \dot{v}\end{pmatrix} = \varepsilon\begin{pmatrix}-\frac{\delta}{2} & \frac{\sigma}{2\omega} - \frac{p}{4\omega}\\ -\frac{\sigma}{2\omega} - \frac{p}{4\omega} & -\frac{\delta}{2}\end{pmatrix}\begin{pmatrix}u\\ v\end{pmatrix} + \varepsilon\begin{pmatrix}-\frac{2A\beta u\sqrt{u^2+v^2}}{3\omega\pi} - \frac{2A\gamma v\sqrt{u^2+v^2}}{3\omega\pi}\\ -\frac{2A\beta v\sqrt{u^2+v^2}}{3\omega\pi} + \frac{2A\gamma u\sqrt{u^2+v^2}}{3\omega\pi}\end{pmatrix}. \tag{29}$$

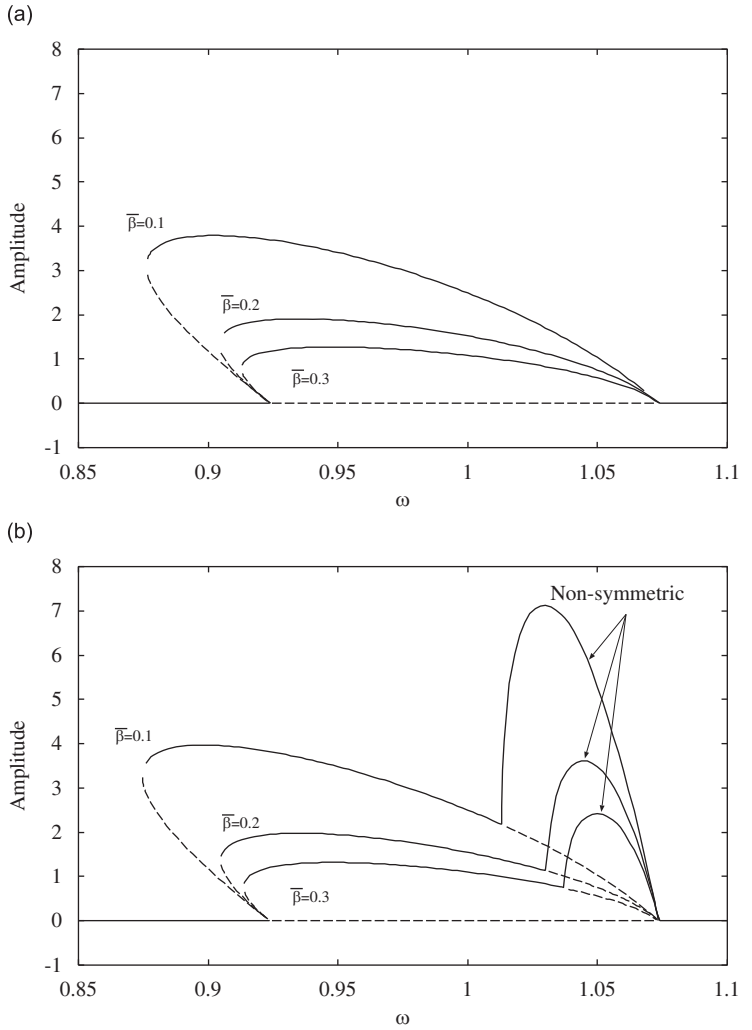

Fig. 2. Effects of shape parameter $\bar{\beta}$ in softening hysteretic system: $\bar{\gamma}=0.1$, $\bar{\delta}=0$, $\bar{p}=0.3$, $A=0.95$, $k=0.05$. (a) Multiple scale analysis, (b) numerical integration. ——, stable; – – – –, unstable.

The eigenvalues of the first term of the right-hand side of Eq. (29) are

$$\lambda=\frac{-\delta\pm\sqrt{p^2-4\sigma^2}}{4\omega}. \tag{30}$$

When $\delta>0$, the trivial solution is stable for $|\sigma|>\sqrt{p^2-\delta^2}/2$ (two negative real eigenvalues or a pair of complex eigenvalues) and unstable for $|\sigma|<\sqrt{p^2-\delta^2}/2$ (positive and negative real eigenvalues).

When $\delta=0$, the trivial solution is unstable for $|\sigma|<p/2$ (one positive and one negative eigenvalues). When $\delta=0$ and $|\sigma|>p/2$, the system has a pair of complex eigenvalues and the stability cannot be determined by the eigenvalues. Therefore, the next transformation from (u,v) to (r,ϕ) is introduced which corresponds to the solution of linear parts of Eq. (29):

$$\begin{pmatrix}u\\v\end{pmatrix}=\begin{pmatrix}r\sqrt{2\sigma-p}\cos(\Omega t+\phi)\\-r\sqrt{2\sigma+p}\sin(\Omega t+\phi)\end{pmatrix}, \tag{31}$$

where

$$\Omega = \frac{1}{4\omega}\sqrt{4\sigma^2 - p^2}. \tag{32}$$

Substituting Eq. (31) into Eq. (29) yields

$$\dot{r} = -\frac{\varepsilon\delta}{2}r - \frac{2\varepsilon A}{3\omega\pi}\sqrt{2\sigma - p\cos(2\Omega t + 2\phi)}\left\{\beta - \frac{\gamma p}{\sqrt{4\sigma^2 - p^2}}\sin(2\Omega t + 2\phi)\right\}r|r|, \tag{33}$$

$$\dot{\phi} = \frac{\varepsilon}{4\omega}\sqrt{4\sigma^2 - p^2} - \frac{2\varepsilon A\gamma}{3\pi\omega}\frac{\sqrt{2\sigma - p\cos(2\Omega t + 2\phi)}^3}{\sqrt{4\sigma^2 - p^2}}|r|. \tag{34}$$

Averaging the right-hand side of Eq. (33) and substituting $s^2 = |r|$ gives

$$\dot{s} = -\frac{\varepsilon\delta}{4}s - \frac{\varepsilon A\beta}{3\omega\pi}I(\sigma, p)s^3, \tag{35}$$

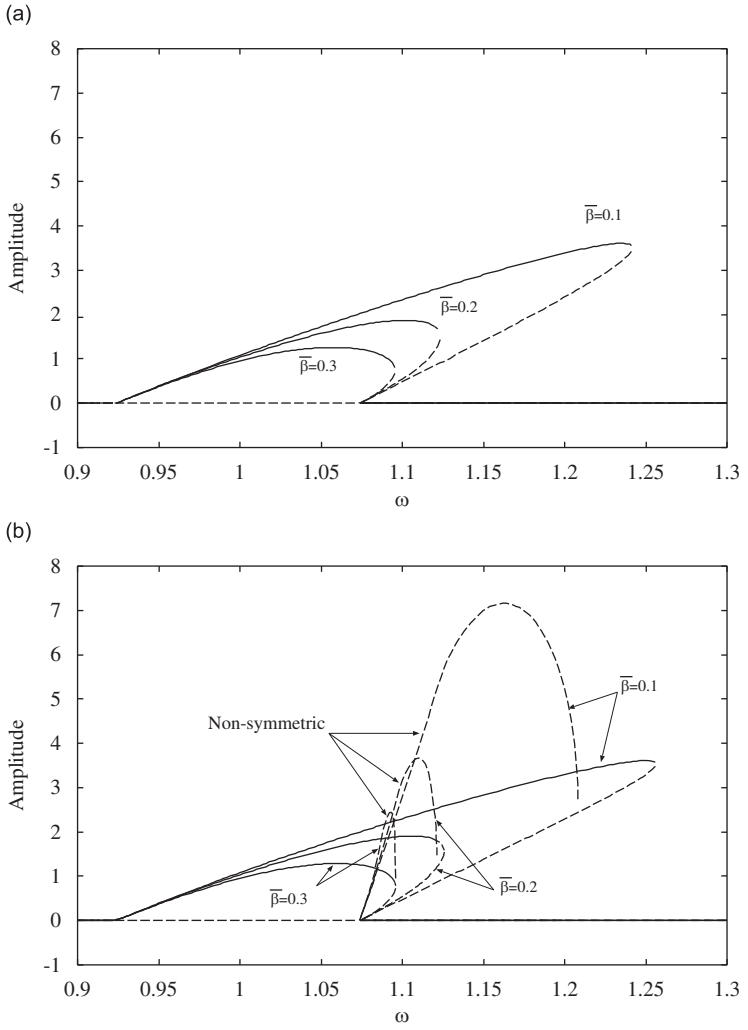

Fig. 3. Effects of shape parameter $\bar{\beta}$ in hardening hysteretic system: $\bar{\gamma} = -0.3$, $\bar{\delta} = 0$, $\bar{p} = 0.3$, $A = 0.95$, $k = 0.05$. (a) Multiple scale analysis, (b) numerical integration. ——, stable; – – – –, unstable.

where

$$I(\sigma,p)=\frac{\Omega}{\pi}\int_0^{\pi/\Omega}\sqrt{2\sigma-p\cos(2\Omega t+2\phi)}\,\mathrm{d}t. \tag{36}$$

From Eq. (35), $\delta=0$ is shown to be a Hopf bifurcation [24] point. As a result, the trivial solution is asymptotically stable even when $\delta=0$. This is due to the hysteretic restoring force characteristics.

It is noted that the system (29) undergoes codimension 1 bifurcation when $\delta>0$ and $|\sigma|=\sqrt{p^2-\delta^2}/2$ and codimension 2 bifurcation when $\delta=0$ and $|\sigma|=p/2$. These bifurcations cannot be analyzed by the present analysis because the analysis is limited to symmetric approximate solutions and non-symmetric solutions need to be considered to deal with the bifurcations as will be described in Section 5.

5. Numerical integration

Resonance curves obtained by both the second-order multiple scale analysis and the numerical integration of Eqs. (1) and (2) are compared to examine the validity of the analysis and the stability and bifurcations of the system are discussed.

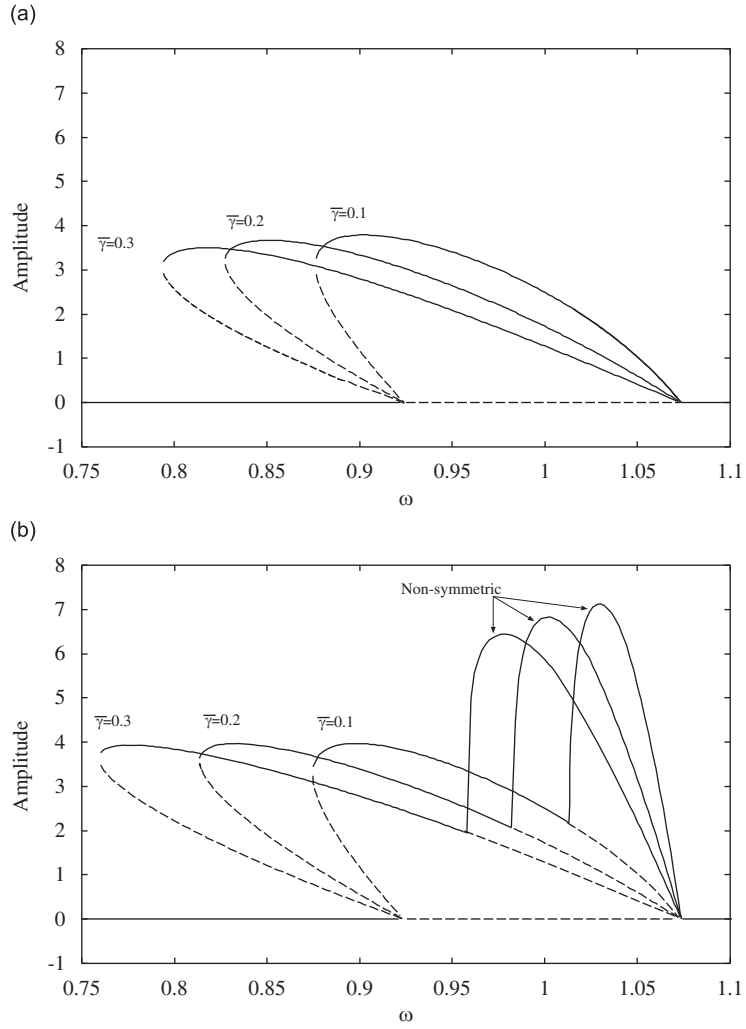

Fig. 4. Effects of shape parameter $\bar{\gamma}$ in softening hysteretic system: $\bar{\beta}=0.1$, $\bar{\delta}=0$, $\bar{p}=0.3$, $A=0.95$, $k=0.05$. (a) Multiple scale analysis, (b) numerical integration. ——, stable; – – – –, unstable.

In the following results, $A = 0.95$ and $k = 0.05$ are used to consider the case that the hysteretic restoring force is predominant over the linear one and $\bar{\delta} = 0, 0.05, 0.1$ and $\bar{p} \leqslant 0.5$ for weak damping and excitation.

5.1. Resonant characteristics

Figs. 2 and 3 show the effects of β on the resonant characteristics of the softening and hardening systems, respectively. Figs. 2(a) and 3(a) shows the result of the second-order multiple scale analysis and Figs. 2(b) and 3(b) the results of numerical integration. Horizontal and vertical axes represent ω, which is a half of the excitation frequency, and the amplitude of steady-state response, respectively. Solid and dashed lines represent stable and unstable solutions, respectively.

In the results of the multiple scale analysis as well as the numerical integration, there exist the regions where the trivial solution is unstable, which is similar to Mathieu's equation. Unlike Mathieu's equation, the responses are bounded because non-trivial symmetric periodic solutions exist. The branches of the symmetric solutions have saddle-node bifurcation points. In the numerical integration, further bifurcations are confirmed. At the right ends of the unstable regions of the trivial solution, not only the symmetric periodic solutions but also non-symmetric solutions appear. The non-symmetric solutions diverge in pairs because the system is symmetric. The maximum displacement of one of the pair in the steady state is shown in Figs. 2(b) and 3(b).

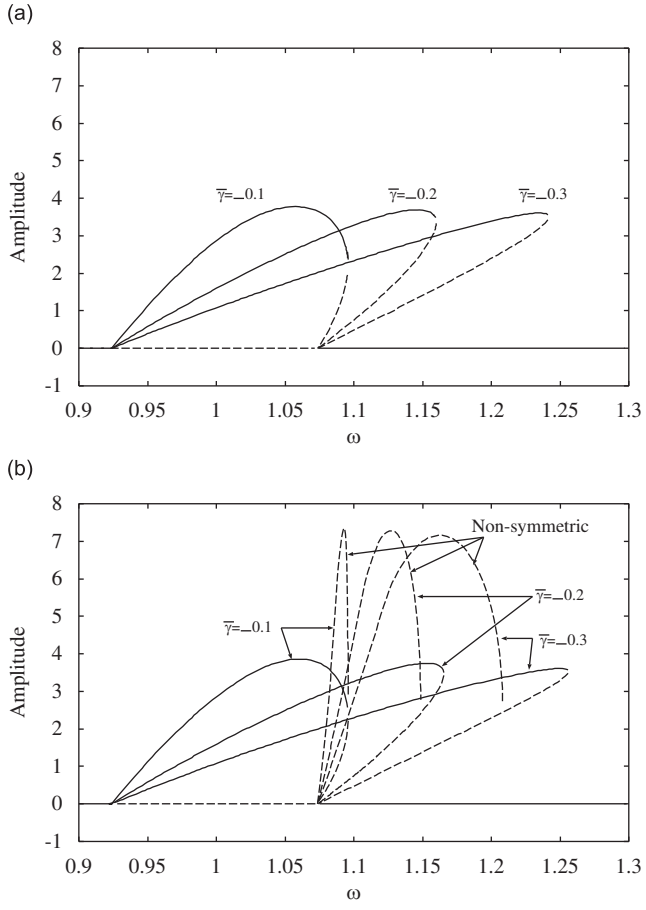

Fig. 5. Effects of shape parameter $\bar{\gamma}$ in hardening hysteretic system: $\bar{\beta} = 0.1$, $\bar{\delta} = 0$, $\bar{p} = 0.3$, $A = 0.95$, $k = 0.05$. (a) Multiple scale analysis, (b) numerical integration. ——, stable; – – – –, unstable.

5.2. Effects of hysteretic loop parameters

In Figs. 2 and 3, β increases, the amplitude of non-trivial solutions decreases while the unstable regions of the trivial solutions remain unchanged in both softening and hardening systems. Figs. 4 and 5 shows the effects of γ on the resonant characteristics of the softening and hardening systems, respectively. Figs. 4(a) and 5(a) show the results of the second-order multiple scale analysis and Figs. 4(b) and 5(b) show the results of numerical integration. As $|\gamma|$ increases, the slopes of resonant curves decrease while the amplitude of the non-trivial solutions remain almost constant in both softening and hardening systems.

5.3. Effects of excitation amplitude and damping

Figs. 6 and 7 show the effects of excitation amplitude p and damping coefficient δ on resonant characteristics in the softening and hardening hysteretic systems, respectively. As p increases or δ decreases, the unstable region of trivial solution enlarges and the amplitude of non-trivial solution increases, which is similar to Mathieu's equation. Aforementioned bifurcations remain when $\delta > 0$.

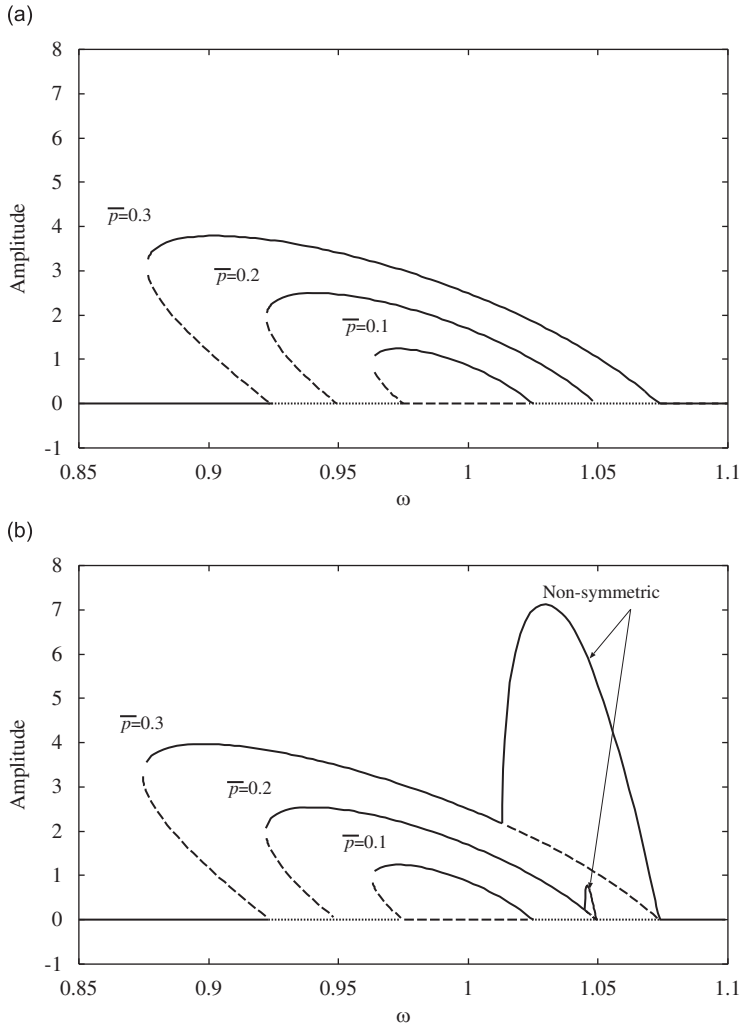

Fig. 6. Effects of excitation amplitude $\bar{p}$: $\bar{\beta} = 0.1$, $\bar{\gamma} = 0.1$, $\bar{\delta} = 0$, $A = 0.95$, $k = 0.05$. (a) Multiple scale analysis, (b) numerical integration. ——, stable; – – – –, unstable.

5.4. Stability regions

Stability regions of different stable and unstable solutions in $\omega-p$ plane for softening and hardening hysteretic systems are illustrated in Figs. 8 and 9, respectively. Solid lines display stability boundaries by numerical integration and dashed lines display theoretical stability boundaries of trivial solution described with Eq. (30).

In the case of softening hysteretic system (Fig. 8), trivial solution is stable in regions I, IV and III. Although the trivial solution becomes unstable in regions II and V as in the case of Mathieu equation, a stable symmetric periodic solution exists across regions II and IV. The solution coexists with an unstable solution in region IV because of saddle-node bifurcation. In region V where excitation amplitude p is large inside the region II, the stable symmetric solution becomes unstable and a pair of stable non-symmetric periodic solutions are generated.

In the case of hardening hysteretic system (Fig. 9), similar characteristics are found. The trivial solution is stable in regions I, III, IV and V and unstable in region II. Stable symmetric periodic solution exists across regions II, IV and V and coexists with unstable symmetric solution in regions IV and V. A pair of unstable non-symmetric periodic solutions exists in region V.

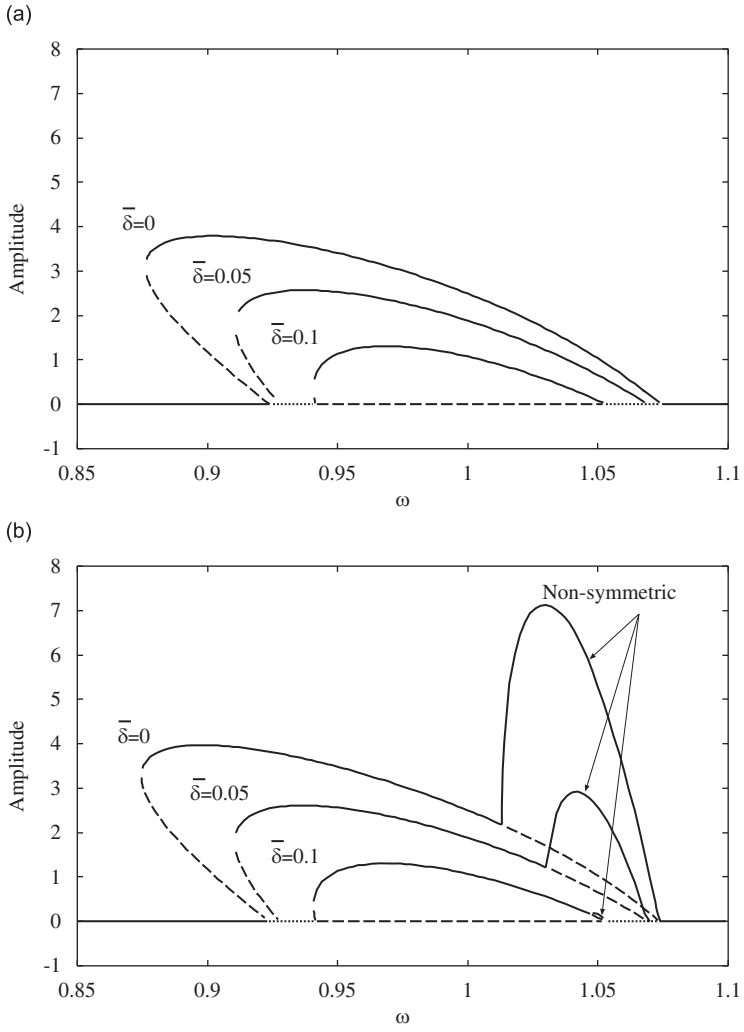

Fig. 7. Effects of damping coefficient $\bar{\delta}$: $\bar{\beta}=0.1$, $\bar{\gamma}=0.1$, $\bar{p}=0.3$, $A=0.95$, $k=0.05$. (a) Multiple scale analysis, (b) numerical integration. ——, stable; – – – –, unstable.

Similar to other nonlinear parametric systems, hysteretic nonlinearity can limit the response and generate periodic solutions in principal resonance region. However, chaotic or quasi-periodic solution which is observed in other nonlinear systems cannot be found in the present hysteretic systems.

5.5. Comparison with the analytical results

Concerning the unstable regions of the trivial solution and the amplitude and saddle-node bifurcation point of the non-trivial symmetric periodic solution, fairly good agreement is found between the results of the second-order multiple scale analysis and the numerical integration. Stability analysis described in Section 4.4 explains the reason why the unstable region of the trivial solution is independent of β and γ. Analytical explanation of the bifurcation by which non-symmetric periodic solutions appear is the subject in future.

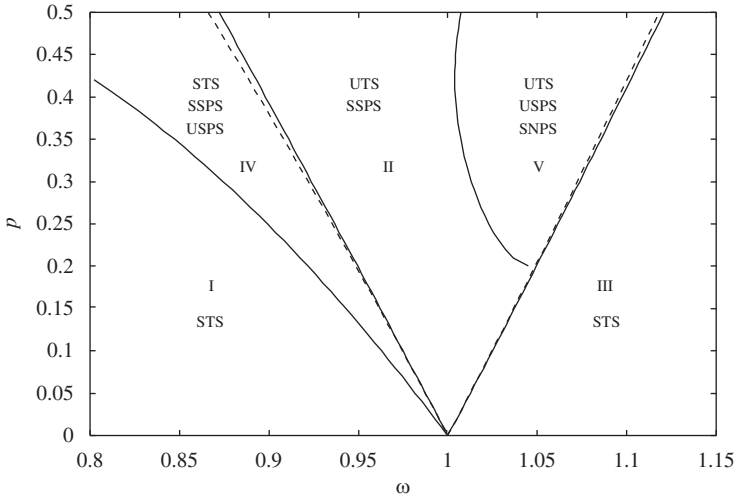

Fig. 8. Regions of different types of solutions in softening system: $\bar{\beta} = 0.1$, $\bar{\gamma} = 0.1$, $A = 0.95$, $k = 0.05$, STS, stable trivial solution; UTS, unstable trivial solution; SSPS, stable symmetric periodic solution; USPS, unstable symmetric periodic solution; SNPS, a pair of stable non-symmetric periodic solutions; ——, numerical; – – – –, theory.

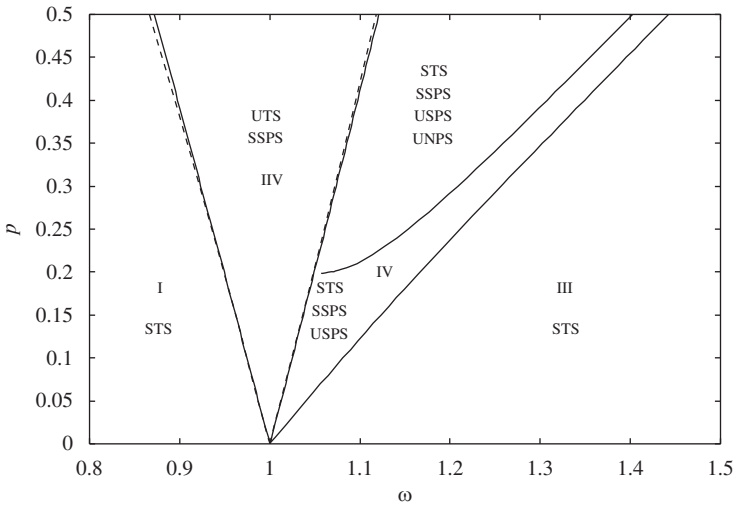

Fig. 9. Regions of different types of solutions in hardening system: $\bar{\beta} = 0.1$, $\bar{\gamma} = -0.3$, $A = 0.95$, $k = 0.05$. STS, stable trivial solution; UTS, unstable trivial solution; SSPS, stable symmetric periodic solution; USPS, unstable symmetric periodic solution; SNPS, a pair of stable non-symmetric periodic solutions; UNPS, a pair of unstable non-symmetric periodic solutions; ——, numerical; – – – –, theory.

6. Conclusion

Nonlinear vibrations of a smooth hysteretic systems subjected to principal parametric harmonic excitation was investigated. As a model for hysteresis, Wen's differential equation was used. By employing the piecewise power series expression for hysteretic restoring force, the method of multiple time scales was applied to obtain the second-order approximate solutions and their stability. Numerical integration was also performed so as to illustrate the stability and bifurcations of the system. The conclusions are summarized as follows:

(1) Independently of the extent of viscous damping, the trivial solution is asymptotically stable outside the principal resonance region due to Hopf bifurcation.
(2) The trivial solution is unstable inside the principal resonance region but the response is bounded because non-trivial periodic solutions exist.
(3) The unstable region of trivial solution is dependent on detuning, amplitude of excitation and damping and independent of hysteretic loop characteristics.
(4) Saddle-node bifurcation of non-trivial symmetric periodic solution occurs in both softening and hardening systems.
(5) There exists the bifurcation by which a pair of non-symmetric solutions diverge from non-trivial symmetric solution.
(6) The validity of the present analysis was confirmed concerning the stability of the trivial solution and the amplitude of symmetric periodic solution.

References

[1] T.K. Caughey, Sinusoidal excitation of a system with bilinear hysteresis, *Transactions of ASME, Journal of Applied Mechanics* 27 (1960) 640–643.
[2] D. Capecchi, Periodic response and stability of hysteretic oscillators, *Dynamics and Stability of Systems* 6 (2) (1991) 89–106.
[3] C. Wong, Y.Q. Ni, S.L. Lau, Steady-state oscillation of hysteretic differential model. I: response analysis, *ASCE, Journal of Engineering Mechanics* 120 (11) (1994) 2271–2298.
[4] N. Okuizumi, K. Kimura, Multiple time scale analysis of hysteretic systems subjected to harmonic excitation, *Journal of Sound and Vibration* 272 (2004) 675–701.
[5] C.Y. Yang, A.H.-D. Cheng, R.V. Roy, Chaotic and stochastic dynamics for a nonlinear structural system with hysteresis and degradation, *Probabilistic Engineering Mechanics, Part 2* 6 (3/4) (1991) 193–203.
[6] W.K. Tso, K.G. Asmis, Parametric excitation of a pendulum with bilinear hysteresis, *Transactions of ASME Journal of Applied Mechanics* (1970) 1061–1068.
[7] B. Poddar, F.C. Moon, S. Mukherjee, Chaotic motion of an elastic plastic beam, *Transactions of ASME Journal of Applied Mechanics* 55 (1988) 185–189.
[8] R. Pratap, S. Mukherjee, F.C. Moon, Dynamic behaviour of a bilinear hysteretic elasto-plastic oscillator, part I: free oscillations, *Journal of Sound and Vibration* 172 (3) (1994) 321–337.
[9] R. Pratap, S. Mukherjee, F.C. Moon, Dynamic behavior of a bilinear hysteretic elasto-plastic oscillator, part II: oscillations under periodic impulse forcing, *Journal of Sound and Vibration* 172 (3) (1994) 339–358.
[10] R. Pratap, P. Holmes, Chaos in a mapping describing elastoplastic oscillations, *Nonlinear Dynamics* 8 (1995) 111–139.
[11] J.R. Boston, Response of a nonlinear form of the Mathieu equation, *Journal of the Acoustical Society of America* 49 (1) (1970) 299–305.
[12] E. Esmailzadeh, G. Nakhaie-Jazar, Periodic solution of a Mathieu–Duffing type equation, *International Journal of Non-Linear Mechanics* 32 (5) (1997) 905–911.
[13] M. Mond, G. Cederbaum, Stability analysis of the non-linear Mathieu equation, *Journal of Sound and Vibration* 167 (1) (1993) 77–89.
[14] W. Szamplinska-Stupnicka, R.H. Plaut, J.-C. Hsieh, Period doubling and chaos in unsymmetric structures under parametric excitation, *Transactions of the ASME, Journal of Applied Mechanics* 56 (1989) 947–952.
[15] L.D. Zavodney, A.H. Nayfeh, The response of a single-degree-of-freedom system with quadratic and cubic non-linearities to a fundamental parametric resonance, *Journal of Sound and Vibration* 120 (1) (1988) 63–93.
[16] L.D. Zavodney, A.H. Nayfeh, N.E. Sanchez, The response of a single-degree-of-freedom system with quadratic and cubic non-linearities to a principal parametric resonance, *Journal of Sound and Vibration* 129 (3) (1989) 417–442.
[17] R.W. Leven, B.P. Koch, Chaotic behaviour of a parametrically excited damped pendulum, *Physics Letters* 86A (2) (1981) 71–74.
[18] R.W. Leven, B. Pompe, C. Wilke, B.P. Koch, Experiments on periodic and chaotic motions of a parametrically forced pendulum, *Physica D* 16 (1985) 371–384.
[19] M.J. Clifford, S.R. Bishop, Generic features of escape from a potential well under parametric excitation, *Physics Letters A* 184 (1993) 57–63.

[20] M.J. Clifford, S.R. Bishop, Approximating the escape zone for the parametrically excited pendulum, *Journal of Sound and Vibration* 172 (4) (1994) 572–576.
[21] Y.K. Wen, Method for random vibration of hysteretic systems, *ASCE, Journal of Engineering Mechanics* 102 (EM2) (1976) 249–263.
[22] T.T. Baber, Y.K. Wen, Random vibration of hysteretic, degrading systems, *ASCE, Journal of Engineering Mechanics* 107 (EM6) (1981) 1069–1087.
[23] A.H. Nayfeh, D.T. Mook, *Nonlinear Oscillations*, Wiley, New York, 1979.
[24] S. Wiggins, *Introduction to Applied Nonlinear Dynamical Systems and Chaos*, Springer, Berlin, 1990.